
Implicit Delta Learning of High Fidelity Neural Network Potentials

Stephan Thaler*
Valence Labs

Cristian Gabellini*
Valence Labs

Nikhil Shenoy
Valence Labs

Prudencio Tossou†
Valence Labs

Abstract

Neural network potentials (NNPs) offer a fast and accurate alternative to *ab-initio* methods for molecular dynamics (MD) simulations but are hindered by the high cost of training data from high-fidelity Quantum Mechanics (QM) methods. Our work introduces the *Implicit Delta Learning* (IDLe) method, which reduces the need for high-fidelity QM data by leveraging cheaper semi-empirical QM computations without compromising NNP accuracy or inference cost. IDLe employs an end-to-end multi-task architecture with fidelity-specific heads that decode energies based on a shared latent representation of the input atomistic system. In various settings, IDLe achieves the same accuracy as single high-fidelity baselines while using up to 50x less high-fidelity data. This result could significantly reduce data generation cost and consequently enhance accuracy and generalization, and expand chemical coverage for NNPs, advancing MD simulations for material science and drug discovery. Additionally, we provide a novel set of 11 million semi-empirical QM calculations to support future multi-fidelity NNP modeling.

1 Introduction

Molecular dynamics (MD) simulations are a major computational workhorse in material science and drug discovery, enabling the *in-silico* study of molecular systems and their dynamics. The accuracy of an MD simulation is determined by the potential energy function, which defines intra- and intermolecular forces. *Ab-initio* MD simulations employ forces computed from first-principles quantum mechanics (QM) methods such as density functional theory (DFT). While highly accurate, the unfavorably scaling cost of QM computations hinders the application of *ab-initio* MD simulations for large systems or long timescales.

In recent years, neural network potentials (NNPs) [1–5] have enabled orders of magnitude faster MD simulations with *ab-initio* accuracy [6, 7]. However, practical issues prevent their widespread development and adoption. The first issue is the large amount of high-fidelity (HF) QM data needed for training. Collecting this data is expensive and limited in terms of chemical coverage and size, resulting in fewer NNPs being developed. The second issue is the limited generalization capability of NNPs. Due to data limitations, NNPs often fail to generalize to unseen parts of chemical space [8–10]. To improve the stability and accuracy of NNP-based MD simulations, prior potentials [11, 12, 6], MD observable-based training [13, 14], and/or NNP fine-tuning with additional QM data [10, 15, 16] are often required. To enhance the development and adoption of NNPs, it is imperative to lower the data generation costs for their initial training and fine-tuning.

One approach to reduce NNP training and fine-tuning costs is to leverage lower-fidelity (LF) methods such as Tight-Binding (TB) (e.g., GFN2-xTB [17], DFTB3[18]) or Hartree-Fock-based Semi-Empirical (SE) methods (e.g., PM6 [19]). These methods are significantly less expensive, though less

*These authors contributed equally to this work.

†Reachout at: prudencio at valencelabs.com

accurate and generalizable, compared to high-fidelity (HF) computations such as DFT or coupled cluster. The aim is to increase NNP stability, generalization, and chemical space coverage without sacrificing accuracy or requiring additional fine-tuning. Δ -learning methods train ML models to predict the energy difference between an LF and a HF method [20, 21, 10, 22]. The underlying idea is that learning the difference Δ is more data efficient than directly predicting the HF energy. However, while this reduces the number of HF labels needed during training, it significantly increases inference cost due to on-the-fly LF QM calculations during MD simulations.

In this work, we propose the *Implicit Delta Learning* (IDLe) training strategy to lower the training cost of NNPs and increase their data efficiency, chemical coverage, and generalization without requiring additional QM computations at inference. Based on a multi-task network, IDLe reduces the number of HF labels by replacing them with LF labels (typically SE labels) and implicitly learning to decode the HF energy from a shared latent representation of the input system. Our contributions can be summarized as follows:

1. We propose the *IDLe* training strategy to replace the majority of HF training data required by HF NNPs with LF data. Consequently, IDLe can reduce the cost of NNP training data generation by orders of magnitude, even requiring no additional HF labels in certain cases.
2. We showcase IDLe’s generalization effectiveness within and outside the training distribution for NNPs trained on various QM datasets relevant to drug discovery (QMugs [23], Spice [24, 25], QM7-X [26], ANI1-ccx [27]), spanning multiple combinations of HF and LF methods.
3. We performed ~ 11 million single point energy computations using LF QM methods to augment existing datasets and demonstrate the power of IDLe. These new computations will be publicly available to foster further research into multi-fidelity NNP training and IDLe.

2 Related works

Δ -learning: Given that LF methods capture many interaction terms of HF methods, "explicit" Δ -learning aims to predict the remaining Δ using ML models. During training, samples are labeled with both LF and HF methods, and during inference, LF labels are computed and added to the predicted Δ s to obtain the HF energy. Since Δ s are easier to learn, Δ -models are data-efficient and highly accurate during inference at a cost comparable to that of the LF computation.

The concept of Δ -learning in quantum chemistry was introduced by Ramakrishnan et al. [20], who demonstrated its data efficiency compared to direct HF learning. Their Δ -models learned and predicted differences in levels of theory (e.g., PM6 \rightarrow CCSD(T)), across quantum properties (e.g., energy \rightarrow enthalpy), and geometries. Later, Boselt et al. [28] and Hofstetter et al. [29] applied Δ -learning to incorporate long-range interactions in their NNPs for condensed-phase and reactive systems by learning the energy differences between DFT and SE methods. DelFTa [23] predicts a wide array of quantum properties by Δ -learning from GFN2-xTB to ω B97X-D/def2-SVP.

High-fidelity NNPs at low cost: While Δ -learning reduces training data costs, its inference cost is high for most applications. Consequently, alternatives such as active learning [15, 30, 31], transfer learning [32], meta-learning [33], and multi-task pre-training [34] aim to minimize the amount of HF training data while avoiding increased inference cost.

Active learning (AL) collects the most informative HF data based on the NNP predictive uncertainty, significantly reducing training data size [15, 30, 31]. For example, ANI-1x [35, 36], built with AL, has ~ 4 x less DFT data than ANI-1 [37], yet training NNPs on ANI-1x yields superior performance.

Transfer learning methods use cheap LF data to pre-train an NNP and fewer HF calculations for fine-tuning. For example, Smith et al. [32] pre-trained an NNP on ~ 5 million DFT points before fine-tuning with 0.5 million CCSD(T)* samples. Similar transfer learning applications typically transfer representations within the same part of chemical space, transferring from rather costly methods such as DFT or Hartree-Fock to higher-fidelity methods as the target [38–42]. However, transfer learning NNPs based on cheap SE methods has not yet been attempted, despite very recent applications in molecular property prediction [43, 44] and earlier work using "synthetic data" [45]. Transfer learning has two stages, is not end-to-end, and can require extensive training computations

if both the LF and the HF data are sizable. Selecting the pre-training dataset to transfer from for a given HF target can also be daunting.

Meta-learning [33] and multi-task networks [34] can also be used for pre-training, learning from different parts of chemical space using multiple QM datasets before fine-tuning to a specific HF QM method or domain of chemical space. They share the same limitations as transfer learning methods.

Multi-fidelity QM datasets: Numerous QM datasets have been created for NNP training, but only a few include multi-fidelity QM labels that improve training efficiency for HF NNPs. The largest is PubChemQC [46], which contains DFT (B3LYP/6-31G*) and SE (PM6) properties for ~ 86 million geometries covering a wide range of molecules. Similarly, QMugs [23] includes ~ 2 million conformations from 665,000 molecules with up to 100 heavy atoms, providing DFT (ω B97M-D/def2-SVP) and TB (GFN2-xTB) energies and properties. The QM7-X dataset [26] and MultiXC-QM9 [47] cover smaller molecules with restricted chemical diversity. QM7-X contains DFT (PBE+MBD) and TB (DFTB3+) energy labels for ~ 4 million conformations of molecules with up to seven heavy atoms. MultiXC-QM9 provides multi-fidelity data with 72 DFT functionals and a TB method (GFN2-xTB). None of these datasets overlap in chemical space or feature the same HF QM method pairs, limiting the study of extrapolation in multi-fidelity or Δ -learning NNPs.

3 Methods

3.1 Preliminaries

NNPs can be trained by minimizing an energy-matching mean squared error (MSE) loss function [1]. For high-fidelity NNPs, we have

$$\mathcal{L} = \frac{1}{N} \sum_{i=1}^N \left[E_i^{\text{HF}} - \hat{E}_{\theta}^{\text{HF}}(\mathbf{S}_i) \right]^2, \quad (1)$$

where \mathbf{S}_i is a conformation of a molecule with K_i atoms, typically represented by positions $\mathbf{R}_i \in \mathbb{R}^{K_i \times 3}$ and atomic numbers $\mathbf{Z}_i \in \mathbb{N}^{K_i}$, E_i^{HF} is the target HF energy, and $\hat{E}_{\theta}^{\text{HF}}(\mathbf{S}_i)$ is the predicted energy of the NNP parameterized by θ .

Instead of directly learning and predicting the HF energy $\hat{E}_{\theta}^{\text{HF}}(\mathbf{S}_i)$, the Δ -learning method [20] learns to predict the energy difference with respect to a LF energy E^{LF} . At inference, predicting the HF energy requires the computation of E^{LF} and the Δ , i.e., $\hat{E}_{\theta}^{\text{HF}}(\mathbf{S}_i) = E_i^{\text{LF}} + \Delta \hat{E}_{\theta}^{\text{HF-LF}}(\mathbf{S}_i)$. The parameters of the Δ -model are learned by minimizing the MSE loss function using samples where we have both the HF and LF labels as $\mathcal{L}^{\Delta} = \frac{1}{N} \sum_{i=1}^N \left[(E_i^{\text{HF}} - E_i^{\text{LF}}) - \Delta \hat{E}_{\theta}^{\text{NN}}(\mathbf{S}_i) \right]^2$. Due to the form of this loss, we need pairs of HF and LF energies for any given geometry in our training data, which makes data collection quite expensive. Additionally, Δ -learning methods are straightforward to apply for datasets with one LF and one HF method, but generalizing them to multiple LF methods and a HF one seems challenging.

3.2 Implicit Delta Learning

To mitigate the limitations of existing learning approaches when leveraging LF data to improve the data efficiency and accuracy of HF NNPs, we propose the Implicit Delta Learning training approach, named IDLe. In comparison to Δ -learning, IDLe can generalize easily to multiple low-fidelity methods and does not need LF computations to be very accurate during inference. Relative to transfer learning methods, it is an end-to-end approach that leverages LF and HF data simultaneously instead of the two stages of pre-training and fine-tuning to allow transfer. The full comparison between IDLe and other training approaches for HF NNPs is shown in Table 1.

Technically, IDLe is a multi-task learning approach, where each prediction head corresponds to a different QM method. All prediction heads share the same backbone network, forcing them to decode their respective energy value from a shared latent representation of the input geometry. Due to this framing, one can leverage multiple LF labels to improve HF prediction accuracy.

In order to train a model via IDLe, we minimize the following multi-fidelity multi-task MSE loss function:

$$\mathcal{L}^{MT} = \frac{1}{M} \sum_{i=1}^N \sum_{h=1}^H I_{i,h} \times \left[E_{i,h} - \hat{E}_{\theta,h}(\mathbf{S}_i) \right]^2, \quad (2)$$

where M is the number of energy labels in the dataset, N is the number of geometries, H is the number of QM methods (both LF and HF) considered, $I_{i,h}$ is 0 if the label $E_{i,h}$ is missing, otherwise 1, and $\hat{E}_{\theta,h}(\mathbf{S}_i)$ is the energy prediction of head h for the geometry \mathbf{S}_i .

Table 1: Desiderata fulfillment of different high fidelity NNP training methods.

	Direct-learning	Δ -learning	Active learning	Transfer learning	IDLe
<i>Training data efficiency</i>	\times	\sim	\checkmark	\checkmark	\checkmark
<i>Inference cost</i>	\checkmark	\times	\checkmark	\checkmark	\checkmark
<i>Accuracy</i>	\checkmark	$\checkmark\checkmark$	\checkmark	\checkmark	\checkmark
<i>Leverage LF labels</i>	\times	\sim	\times	\checkmark	\checkmark
<i>OOD generalization</i>	\times	\checkmark	\times	\sim	\checkmark

As the LF energies computation costs are very small compared to the HF ones (especially for larger molecules and expensive HF methods), we assume that for all conformations with HF labels we also have the LF ones. The reverse is not true, which leads to highly different numbers of HF and LF labels during training. The training data efficiency of IDLe compared to direct and Δ -learning stems from using significantly fewer HF compared to LF labels. Under these circumstances, IDLe implicitly learns a shared representation from which HF and LF energies can be decoded, enabling a better chemical coverage for the HF head due to the large number of conformers with only LF labels. In fact, the HF head benefits from the latent representation optimized via the low-fidelity prediction heads, increasing its domain of applicability without requiring further high-fidelity labels. During inference, IDLe simply uses the HF head for predictions, which is significantly cheaper than Δ -learning methods, which need to compute the LF label in addition to the Δ prediction.

3.3 Generating Multi-Fidelity data

To assess the benefits of multiple and varying degrees of LF data on HF-NNP training, we constructed datasets where geometries have at least one HF energy label (DFT, CCSD(T)) and two LF labels: a tight binding (TB) and an SE based on the Hartree-Fock. TB is considered slightly higher fidelity than Hartree-Fock-based SE labels, but both often have the same computational cost for small systems, even if TB is more expensive to scale to large molecules. We expanded existing datasets, covering several parts of chemical space, with LF QM labels, which were fast to compute. The original datasets are the following:

- **ANI1-ccx** [27]: ANI1-ccx has uncharged small molecules covering four elements. The energies are calculated using the CCSD(T)/CBS level of theory. Despite the limited chemical coverage, this dataset will allow the study of the extent to which LF labels can help NNPs to predict the highest fidelity energies.
- **Spice** [24]: SpiceV1, containing originally ~ 1.1 million conformations of small molecules, dimers, dipeptides, and solvated amino acids covering 15 elements. SpiceV2 [25] extends to bulk water systems, solvated molecules, and two more elements. HF energies are calculated using the ω B97M-D3(BJ)/def2-TZVPPD level of theory.
- **QM7-X** [26] contains DFT (PBE+MBD) and TB (DFTB3+) energy labels for ~ 4 million conformations of molecules up to seven heavy atoms.
- **QMugs** [23] has ~ 2 million geometries from 665k molecules with up to 100 heavy atoms and provides DFT (ω B97M-D/def2-SVP) and TB (GFN2-xTB) energy labels.

Table 2 summarizes the QM methods existing in each datasets and the ones we have added. Note that we suffixed each dataset name by "vL" to refer to their new version with added labels. To ensure data consistency, all the computed datasets underwent further processing to detect potential errors from the single point calculations. Any errors identified during this stage underwent a manual recalculation

and subjected to the same post-processing procedure. A few molecular structures were systematically removed after multiple rounds of re-calculation without convergence.

All the calculations were set up using QCSubmit [48] and the computations were managed with QCfractal [49]. The backends for the single point calculations are MOPAC [50] for PM6 and xTB [51] for GFN2-xTB.

Table 2: Summary of the generated datasets with QM methods and number of conformers.

Dataset	Original labels		Added Labels			# Conformers
	High-fidelity QM	TB	DFT	TB	SE	
ANI-1ccxvL	CCSD(T)/CBS		ω B97X-d/def2-svp	GFN2	PM6	489,457
SpicevL2	ω B97M-D3(BJ)/def2-TZVPPD			GFN2	PM6	2,004,893
QM7-XvL	PBE0+MBD	DFTB3+			PM6	4,195,192
QMugsvL	ω B97X-D/def2-SVP	GFN2			PM6	1,992,941

4 Experiments

4.1 Setup

We perform all experiments using TorchMDNet 2.0 [5] with prediction heads consisting of MLPs with a single hidden layer; a detailed list of hyperparameters is provided in Appendix A.1. We compute normalized energy labels \tilde{E} for each dataset and QM level of theory j by subtracting the mean energy value of each atom type as computed by a linear model $\mu_{j,k}$, analogous to [20]. In addition, we scale the energy by the mean residual energy per atom σ_j :

$$\tilde{E}_{i,j}^{\text{QM}} = \frac{1}{\sigma_j} \left(E_{i,j}^{\text{QM}} - \sum_{k=1}^{K_i} \mu_{j,k} \right). \quad (3)$$

For all datasets, we perform a random 80%-10%-10% training-validation-test split. For all the experiments, we vary the amount of HF labels from 1%, 2.5%, 10%, 25% to 100% of the combined training and validation set, but we always evaluate generalization on the full HF test set.

We compare the data efficiency of IDLe to several competing training approaches: direct learning, Δ -learning, and fine-tuning (transfer learning). Direct learning is trained exclusively on the available HF data, serving as a baseline to evaluate the effectiveness of leveraging LF data through IDLe. Δ -learning is used to assess the difference between implicitly and explicitly leveraging the LF energies with respect to predicting the HF labels. Pre-training on SE labels and fine-tuning on the HF data will use the same amount of labels as IDLe, and therefore a comparison will show if any benefits with IDLe are due to the larger amounts of labels or the end-to-end training leading to better latent representations.

4.2 DFT data efficiency

Our first experiment aims to measure IDLe’s effectiveness at leveraging LF labels and compare it with other baselines for within distribution (IID) generalization. Herein, we only use QMugsvL and QM7-XvL and leverage all available LF data while varying the amount of HF data.

Figure 1 gives an overview of the results and circumstances under which SE labels help. For both datasets, at all amounts of DFT data and LF methods, direct learning significantly underperforms relative to other methods, highlighting the benefits of leveraging SE data. For IDLe and fine-tuning approaches, the gap relative to direct learning starts wide in low data settings and shrinks when enough HF data is available. We explain the shrinking gap by the experiment setup herein, which only measures IID generalization. In fact, when the amount of HF increases, IDLe and fine-tuning become closer to direct learning and provide less ability to leverage prior knowledge about geometries compared to direct learning. In other words, in IID settings, the quality of the representation is mostly dictated by the HF labels, but LF ones give useful approximations of those representations in the absence of HF labels. The gap between direct learning and Δ -learning remains consistent as the number of samples increases, as expected. Due to the availability of the SE labels during

inference, Δ -learning becomes easier and more accurate with more samples. However, the quality of the LF labels significantly impacts Δ -learning accuracy. On QMugsvL, Δ -learning with PM6 is significantly less accurate than with GFN2-xTB, and this is confirmed by other experiments (see Figure 3). The quality of the LF method also affects IDLe, which is always better with GFN2-xTB relative to PM6, but to a smaller extent than Δ -learning. Interestingly, using both PM6 and TB labels marginally improves the performance of IDLe. From a QM perspective, these results make sense as the energy difference between DFT methods and PM6 is significantly larger compared to TB methods (GFN2-xTB and DFTB3).

On QMugsvL, IDLe outperforms fine-tuning with a shrinking gap as the number of DFT labels increases. The opposite happens for the QM7-XvL dataset, meaning that more experiments need to be conducted to define the ideal approach in IID settings for a given pair of HF and LF methods. However, it is worth noting that on both datasets, IDLe and fine-tuning approaches reach chemical accuracy (1 kcal/mol) with 4-6x fewer DFT labels than direct learning.

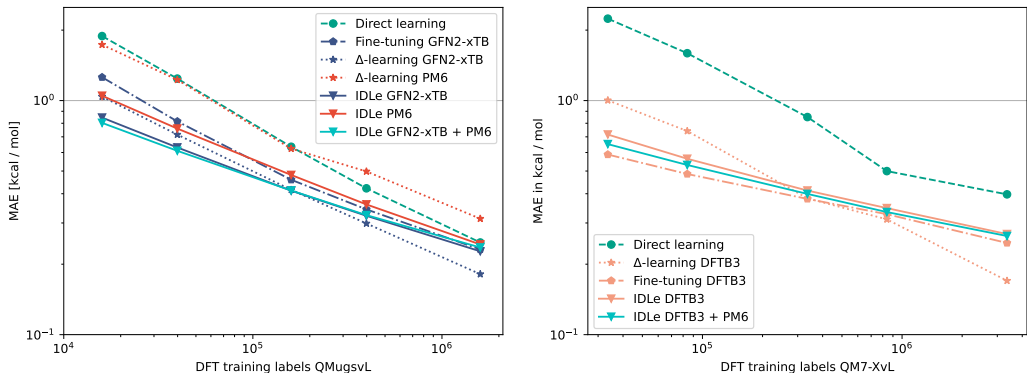


Figure 1: IID performance with DFT as HF labels. We compare of MAE of IDLe with several baselines for a varying amount of DFT labels on QMugs (left) and QM7-X (right).

4.3 Beyond DFT data

Learning to predict the gold-standard coupled cluster CCSD(T) level of theory based on SE or TB methods is a challenging problem [33]. This experiment seeks to address this challenge in an IID setting. Figure 2 shows the generalization performance as the amount of CCSD(T) data seen by the different methods increases. It confirms the superiority of methods leveraging LF labels and their behaviors relative to direct learning, as discussed in Section 4.3. However, herein PM6 together with GFN2-xTB significantly improves the performance of IDLe over GFN2-xTB alone. When adding DFT (ω B97X-d) labels, which are LF and inexpensive compared to CCSD(T) labels, IDLe achieves almost the performance of the 100% data CCSD(T) baseline model using only 2.5% of CCSD(T) labels (40x data efficiency).

Interestingly, even when using GFN2-xTB labels and 1% CCSD(T) labels, fine-tuning and IDLe achieve better MAE than direct learning with 25% CCSD(T) labels. This highlights the enormous advantage of using SE data to significantly reduce the number of required HF labels, even with regards to the most accurate and expensive levels of theory. This hints further that the latent representations learned with the SE methods are truly approximative of the highest quality ones that could be learned with the CCSD(T) energies

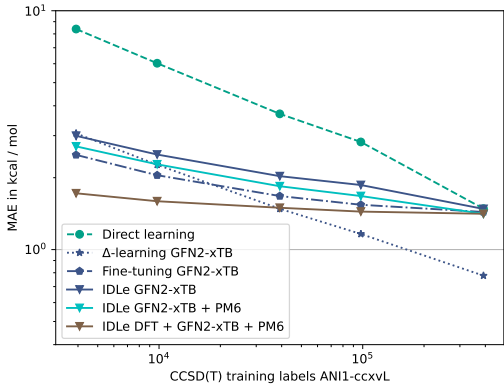


Figure 2: IID performance with CCSD(T) as HF labels: MAE of IDLe compared to several baselines for a varying amount of CCSD(T) labels on ANI1-ccxvL.

themselves. While IDLe combines the directly-learned HF representation with the LF one, fine-tuning can override parts of the LF representation, which seems to be beneficial for GFN2-xTB in this experiment. Hence, we hypothesize that the performance difference between IDLe and transfer learning depends on the amount of mutual information (MI) between the LF and HF labels. IDLe leverages better a high MI, while transfer learning is more robust to low MI due to its ability to unlearn LF representations that are not relevant for HF predictions. That said, since the GFN2-xTB labels themselves contain enough information to allow Δ -learning to achieve chemical accuracy in this extremely difficult setting, we hypothesize that the network capacity might be a limiting factor.

4.4 Out-of-distribution generalization

This section discusses the efficiency of IDLe for varying degrees of distribution shifts that we encounter in practice. For example, given two datasets A and B covering different parts of chemical space and sharing a HF method, a HF NNP trained on A can be intended for usage on B while leveraging all their LF labels. In our experiments, we train with all LF labels of A and B , all HF labels of A and vary the amount of HF labels of B . When this amount is zero, it means that we cannot afford any additional HF computations, so it is a "0-shot learning" setting and an extrapolation to a novel part of the chemical space. This is particularly relevant because there are many molecules for which we can only compute LF labels, but no HF ones (e.g. proteins).

Chemical transferability: Using SpiceV1 and SpiceV1->2 (i.e. the difference between SpiceV2 and SpiceV1) as datasets A and B respectively, we assess the benefits of IDLe in improving chemical transferability out-of-distribution (OOD, see Appendix A.2). Figure 3 (left) shows the average MAE when excluding the PubChem-Boron-Silicon subset of SpiceV1->2, which contains novel chemical elements (B, Si). Without any additional fine-tuning, the direct learning model performs rather poorly compared to all other methods leveraging LF labels. Δ -learning and fine-tuning achieve good 0-shot accuracy, but are outperformed by IDLe using only TB labels. IDLe with TB+ SE labels performs best, achieving the same accuracy as the direct learning baseline with approximately 50% HF labels. Using only 2.5% HF labels and TB+SE labels, IDLe achieves the same accuracy as 100% of Spice1->2, suggesting that the cost associated with expanding SpiceV1 into SpiceV2 could have been reduced significantly by labeling 40x fewer geometries with DFT.

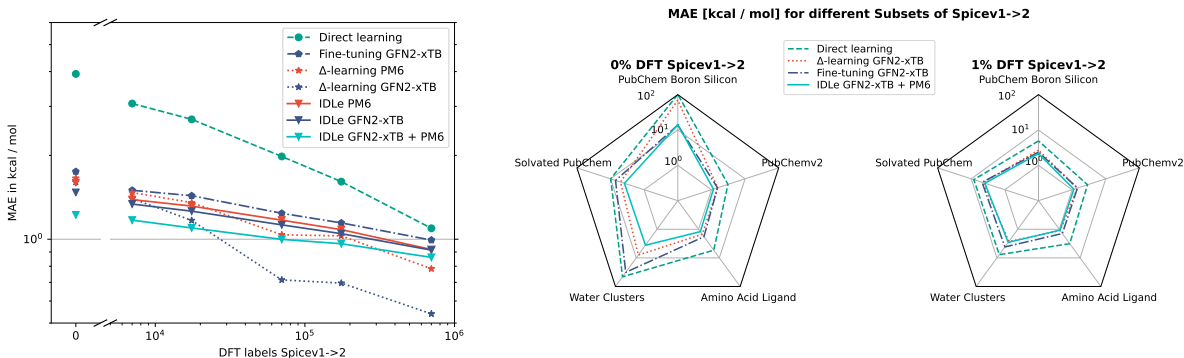


Figure 3: OOD performance on SpiceV2->1 with ω B97M-D3(BJ)/def2-TZVPPD as HF labels: On the left, we show the average MAE of IDLe compared to other methods for a varying amount of DFT labels (without the PubChem-Boron-Silicon subset). On the right, we distinguish between all the subsets of SpiceV1->2 with 0% and 1% of the HF labels available during training.

The MAE on the individual subsets of SpiceV1->2 is shown in Figure 3 (right). For all subsets, in both the 0-shot and 1% DFT label scenarios, IDLe outperforms all the other methods. For the subsets with small to medium distribution shifts (PubChemV2 and Water Clusters), IDLe with TB + SE labels in the 0-shot setting achieves the same accuracy as direct learning with 100% HF labels, circumventing the need for additional DFT data altogether (Appendix A.3). When increasing the number of HF labels in SpiceV1->2, we observe the same trends as on QMugsvL: Δ -learning maintains a rather constant offset to the direct learning baseline, the TB energy performs better than PM6 in both IDLe and Δ -learning, and IDLe with TB + SE labels performs best. The same trends hold for the

PubChem-Boron-Silicon subset (Appendix A.4), but due to the large distribution shift, more HF labels are required with all approaches to reach acceptable MAE values.

Larger molecules: Extrapolation to larger molecules than the ones in the training set is particularly challenging for NNPs. However, it is particularly relevant given the different scaling cost of LF and HF methods with the molecule size. In this experiment, we split QMugsvL into a training dataset A of molecules having up to n_A atoms, and an OOD dataset B of molecules having at least n_B atoms. To simulate increasing levels of OOD difficulty, we perform three splits with $(n_A = 60, n_B = 61)$, $(n_A = 40, n_B = 80)$, and $(n_A = 30, n_B = 120)$.

For all splits, IDLe GFN2-xTB outperforms direct learning and fine-tuning for all amounts of DFT labels on the datasets B . As the distribution shift increases, the need for additional DFT labels increases, as shown by the increasing performance gap between 0% and 1% DFT labels (Figure 4). IDLe leverages the additional HF data most efficiently, reaching almost the same performance as direct learning at 25% DFT labels while using only 1% of them.

4.5 IDLe data scaling and resource gains

Given the IID and OOD results above, IDLe opens new opportunities to build QM datasets to train HF-NNPs by leveraging LF labels more efficiently. Therefore, in this section, we study the computational resource gains from leveraging LF labels with IDLe and its scaling behavior with respect to data.

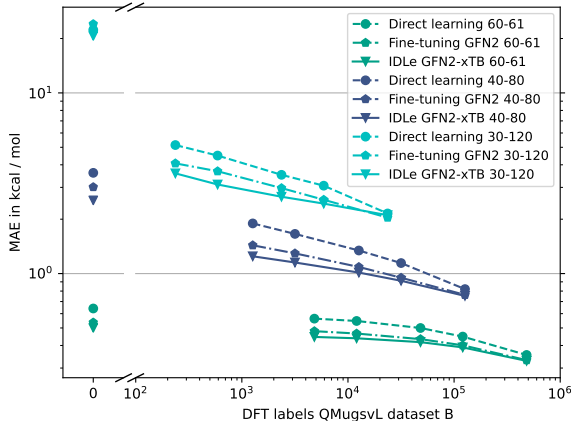


Figure 4: Extrapolation to larger molecules. MAE on datasets B for three different distribution shifts with $(n_A = 60, n_B = 61)$, $(n_A = 40, n_B = 80)$ and $(n_A = 30, n_B = 120)$.

Computational resource gains For a given dataset, let N_{IDLe} represent 1% of the total available HF labels, and N_{direct} be the amount of HF labels needed by direct learning to reach the same performance as IDLe using only 1% of the available HF labels. These quantities can be inferred from Figures 1, 2, and 3. Using the time benchmarks in Appendix A.5, we estimate the CPU time required to generate all HF labels (T_{HF}) and all LF labels (T_{LF}). Table 3 shows the ratios of HF data efficiency ($N_{\text{direct}}/N_{\text{IDLe}}$) and CPU time gains ($N_{\text{direct}} \times T_{\text{HF}} / (0.01 \times T_{\text{HF}} + T_{\text{LF}})$).

These ratios demonstrate that direct learning uses significantly more HF data to achieve the performance that IDLe reaches with only 1% of the HF data. Factoring in the cost of LF labeling, IDLe shows great promise for reducing CPU time for data generation, particularly when dealing with large molecules and when the HF method is much more expensive (and accurate) than the LF method.

Table 3: Cost of generating high fidelity (HF) and tight binding (TB) labels for the whole dataset, as well as IDLe data and compute efficiency ratios compared to direct learning.

Dataset	HF Label		TB Label		Ratios at 1% HF	
	Method	CPU Time [d]	Method	CPU Time [d]	Data	CPU Time [d]
ANI-1ccxvL	CCSD(T)/CBS	6.55e+6	GFN2	170	25x	24.94x
SpicevL2	ω B97M-D3(BJ)/def2-TZVPPD	6.80e+4	GFN2	728	50x	24.15x
QMugsvL	ω B97X-D/def2-SVP	4.36e+4	GFN2	752	5x	1.84x
QM7-XvL	PBE0+MBD	1.21e+4	DFT3B	1487	11.5x	0.87x

IDLe data scaling In many ML domains, including NNPs [52], the IID test loss follows an empirical power-law scaling $\mathcal{L}(R) = \alpha R^{-\beta}$ as a function of resource R (training data, model capacity, compute), where the exponent β is the rate of performance improvement [53–55]. These power laws tend to break down when the model capacity is insufficient for the data size or vice versa [56]. Therefore, we study the scaling laws of IDLe on QMugsvL to determine the limits of increasing the LF or the HF data. We performed this study by fixing the amount of LF data and varying the

amount of HF data (left) and vice versa (right) (see Figure 5). In the former case, the model perfectly follows power-law scaling when increasing HF data up to the amount of LF data. Importantly, the efficiency (β) towards HF data increases with an increasing amount of LF labels. Conversely, when increasing the amount of LF data beyond the amount of HF data, the model enters a "saturation regime" where β decreases as the amount of LF data increases (Figure 5, right). Interestingly, when computing β section-wise (slope of the curve between vertical lines), a secondary trend becomes visible: β increases with an increasing amount of HF labels (Appendix 5).

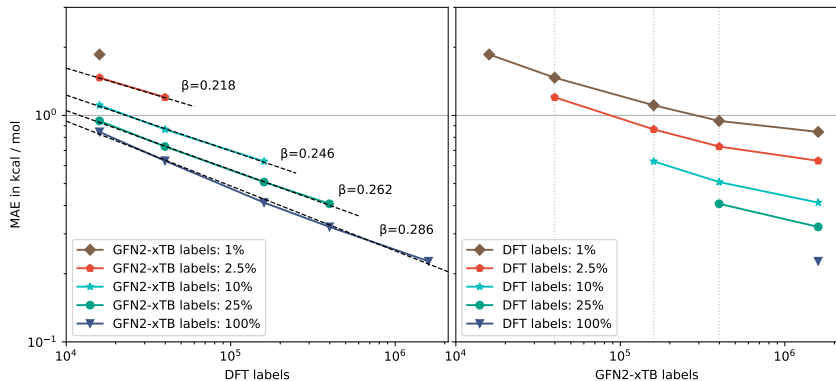


Figure 5: Neural scaling of IDLe. Mean absolute error (MAE) and exponent β on QMugsvL when varying the amount of DFT data for a fixed amount of LF GFN2-xTB data (left) and vice versa (right).

These findings provide insights into the learning behavior of IDLe: when adding new conformations with LF data, the model performs increasingly well in predicting LF energies. However, we hypothesize that the model’s ability to infer HF energies is limited by the size of overlapping representations. Thus, representing LF energies increasingly well exhibits diminishing returns in predicting HF energy (the "saturation regime"). At this point, further increasing the amount of HF labels for existing conformers allows the model to increase the amount of shared representations (up to some limit determined by the specific QM methods involved), enhancing data efficiency for adding more LF conformers.

5 Discussion

We have demonstrated that IDLe can efficiently leverage energy labels from LF QM methods to reduce the number of required HF QM calculations by up to 50x. This significantly lowers the cost of generating QM datasets for larger molecules and broader chemical space coverage, paving the way for foundational NNPs. We envision next-generation NNPs trained on large multi-fidelity QM datasets to enhance the accuracy of MD simulations, supporting material science and drug discovery. Several consistent results emerged from our experiments that are worth highlighting:

- **Increased representation power with multi-fidelity:** Training on multi-fidelity labels via IDLe and transfer learning improves the accuracy compared to direct HF learning by a large margin. For IDLe, this even holds for the case of 100% HF labels, implying more robust representation learning with multi-fidelity labels.
- **Increased OOD Performance with IDLe:** IDLe excels in out-of-distribution (OOD) settings, requiring no additional HF labels for small and medium distribution shifts.
- **Data and training efficiency:** IDLe outperforms Δ -learning in the low data regime and is less sensitive to differences in LF and HF energy values. Unlike Δ -learning, IDLe can improve performance by leveraging multiple LF labels simultaneously. We explain that the enhanced representation capacity is due to the additional LF data. IDLe outperforms or is on par with transfer learning, with IDLe benefiting more strongly from high MI between the LF and HF methods, while transfer learning appears more robust to low MI.

Limitations: In this study, all NNPs were trained via energy-matching. However, training on energies + forces simultaneously is critical to render these models robust and stable during MD simulations

in practice. Additionally, for large OOD distribution shifts, all methods, including IDLe, require a significant amount of HF labels. Nonetheless, IDLe tends to be the most efficient in using these additional HF labels compared to the other methods investigated.

Future work: To address the above limitations, our future studies will focus on training NNPs on energies, forces and other physical quantities. We will explore multiple HF methods with equal importance and study their scaling laws which can guide resource-efficient data generation. The LF data-scaling and their "saturation regime" are of particular interest, as they differ from the scaling laws of transfer learning [57]. Additionally, we will investigate the shared MI between LF and HF methods, providing insights into the NNP latent representations (e.g., GFN2-xTB might have more MI with the ω B97 functionals, while DFTB3 might have less with PBE0+MBD).

References

- [1] Jörg Behler and Michele Parrinello. Generalized Neural-Network Representation of High-Dimensional Potential-Energy Surfaces. *Physical Review Letters*, 98(14):146401, apr 2007. ISSN 00319007. doi:10.1103/PhysRevLett.98.146401.
- [2] Justin Gilmer, Samuel S. Schoenholz, Patrick F. Riley, Oriol Vinyals, and George E. Dahl. Neural Message Passing for Quantum Chemistry. In *Proceedings of the 34th International Conference on Machine Learning*, pages 1263–1272, Sydney, Australia, Aug. 6–11, 2017. ISBN 9781510855144.
- [3] Tsz Wai Ko, Jonas A. Finkler, Stefan Goedecker, and Jörg Behler. A fourth-generation high-dimensional neural network potential with accurate electrostatics including non-local charge transfer. *Nature Communications*, 12:398, dec 2021. ISSN 20411723. doi:10.1038/s41467-020-20427-2.
- [4] Simon Batzner, Albert Musaelian, Lixin Sun, Mario Geiger, Jonathan P Mailoa, Mordechai Kornbluth, Nicola Molinari, Tess E Smidt, and Boris Kozinsky. E(3)-equivariant graph neural networks for data-efficient and accurate interatomic potentials. *Nature Communications*, 13(1): 2453, 2022.
- [5] Raul P Pelaez, Guillem Simeon, Raimondas Galvelis, Antonio Mirarchi, Peter Eastman, Stefan Doerr, Philipp Thölke, Thomas E Markland, and Gianni De Fabritiis. Torchmd-net 2.0: Fast neural network potentials for molecular simulations. *arXiv preprint arXiv:2402.17660*, 2024.
- [6] Albert Musaelian, Simon Batzner, Anders Johansson, and Boris Kozinsky. Scaling the leading accuracy of deep equivariant models to biomolecular simulations of realistic size. In *SC23: International Conference for High Performance Computing, Networking, Storage and Analysis*, pages 1–12. IEEE, 2023.
- [7] Dávid Péter Kovács, J Harry Moore, Nicholas J Browning, Ilyes Batatia, Joshua T Horton, Venkat Kapil, Ioan-Bogdan Magdău, Daniel J Cole, and Gábor Csányi. Mace-off23: Transferable machine learning force fields for organic molecules. *arXiv preprint arXiv:2312.15211*, 2023.
- [8] Xiang Fu, Zhenghao Wu, Wujie Wang, Tian Xie, Sinan Ketten, Rafael Gomez-Bombarelli, and Tommi Jaakkola. Forces are not enough: Benchmark and critical evaluation for machine learning force fields with molecular simulations. In *AI for Science: Progress and Promises Workshop at NeurIPS*, New Orleans, LA, USA, Dec. 2, 2022.
- [9] Stephan Thaler, Gregor Doehner, and Julija Zavadlav. Scalable bayesian uncertainty quantification for neural network potentials: Promise and pitfalls. *Journal of Chemical Theory and Computation*, 19(14):4520–4532, 2023.
- [10] Lin Shen and Weitao Yang. Molecular dynamics simulations with quantum mechanics/molecular mechanics and adaptive neural networks. *Journal of Chemical Theory and Computation*, 14(3): 1442–1455, 2018.
- [11] Jiang Wang, Simon Olsson, Christoph Wehmeyer, Adrià Pérez, Nicholas E. Charron, Gianni De Fabritiis, Frank Noé, and Cecilia Clementi. Machine Learning of Coarse-Grained Molecular Dynamics Force Fields. *ACS Central Science*, 5(5):755–767, 2019. ISSN 23747951. doi:10.1021/acscentsci.8b00913.

- [12] Stephan Thaler, Maximilian Stupp, and Julija Zavadlav. Deep coarse-grained potentials via relative entropy minimization. *The Journal of Chemical Physics*, 157:244103, 2022.
- [13] Stephan Thaler and Julija Zavadlav. Learning neural network potentials from experimental data via differentiable trajectory reweighting. *Nature Communications*, 12(1):6884, 2021. doi:10.1038/s41467-021-27241-4.
- [14] Sanjeev Raja, Ishan Amin, Fabian Pedregosa, and Aditi S Krishnapriyan. Stability-aware training of neural network interatomic potentials with differentiable boltzmann estimators. *arXiv preprint arXiv:2402.13984*, 2024.
- [15] Justin S Smith, Ben Nebgen, Nicholas Lubbers, Olexandr Isayev, and Adrian E Roitberg. Less is more: Sampling chemical space with active learning. *The Journal of Chemical Physics*, 148(24):241733, 2018.
- [16] Cas van der Oord, Matthias Sachs, Dávid Péter Kovács, Christoph Ortner, and Gábor Csányi. Hyperactive learning for data-driven interatomic potentials. *npj Computational Materials*, 9(1):168, 2023.
- [17] Christoph Bannwarth, Sebastian Ehlert, and Stefan Grimme. Gfn2-xtb—an accurate and broadly parametrized self-consistent tight-binding quantum chemical method with multipole electrostatics and density-dependent dispersion contributions. *Journal of Chemical Theory and Computation*, 15(3):1652–1671, 2019.
- [18] Michael Gaus, Qiang Cui, and Marcus Elstner. Dftb3: Extension of the self-consistent-charge density-functional tight-binding method (scc-dftb). *Journal of Chemical Theory and Computation*, 7(4):931–948, 2011.
- [19] James JP Stewart. Optimization of parameters for semiempirical methods v: Modification of nndo approximations and application to 70 elements. *Journal of Molecular Modeling*, 13:1173–1213, 2007.
- [20] Raghunathan Ramakrishnan, Pavlo O Dral, Matthias Rupp, and O Anatole Von Lilienfeld. Big data meets quantum chemistry approximations: the δ -machine learning approach. *Journal of Chemical Theory and Computation*, 11(5):2087–2096, 2015.
- [21] Lin Shen, Jingheng Wu, and Weitao Yang. Multiscale quantum mechanics/molecular mechanics simulations with neural networks. *Journal of Chemical Theory and Computation*, 12(10):4934–4946, 2016.
- [22] Zhuoran Qiao, Matthew Welborn, Animashree Anandkumar, Frederick R Manby, and Thomas F Miller. Orbnet: Deep learning for quantum chemistry using symmetry-adapted atomic-orbital features. *The Journal of Chemical Physics*, 153(12), 2020.
- [23] Isert Clemens, Kenneth Atz, José Jiménez-Luna, and Gisbert Schneider. Qmugs, quantum mechanical properties of drug-like molecules. *Scientific Data* 9(1), June 7, 2022. doi:https://doi.org/10.1038/s41597-022-01390-7.
- [24] Peter Eastman, Pavan Kumar Behara, David L. Dotson, Raimondas Galvelis, John E. Herr, Josh T. Horton, Yuezhi Mao, John D. Chodera, Benjamin P. Pritchard, Yuanqing Wang, Gianni De Fabritiis, and Thomas E. Markland. Spice, a dataset of drug-like molecules and peptides for training machine learning potentials. *arXiv preprint arXiv:2209.10702*, 2022.
- [25] Peter Eastman, Pavan Kumar Behara, David Dotson, Raimondas Galvelis, John Herr, Josh Horton, Yuezhi Mao, John Chodera, Benjamin Pritchard, Yuanqing Wang, Gianni De Fabritiis, and Thomas Markland. Spice 2.0.1, April 2024. URL <https://doi.org/10.5281/zenodo.10975225>.
- [26] Hoja Johannes, Medrano Sandonas Leonardo, Ernst Brian G., Vazquez-Mayagoitia Alvaro, DiStasio Jr. Robert A., and Tkatchenko Alexandre. Qm7-x, a comprehensive dataset of quantum-mechanical properties spanning the chemical space of small organic molecules. *Scientific Data* 43, Vol 8, no.1, 2021/02/02.

- [27] J. S. Smith, R. Zubatyuk, B. Nebgen, N. Lubbers, Barros, A. E. K., Roitberg, O. Isayev, and S. Tretiak. The ani-1ccx and ani-1x data sets, coupled-cluster and density functional theory properties for molecules. *Scientific Data*, 7(1), 134, 2020. doi:https://doi.org/10.1038/s41597-020-0473-z.
- [28] Lennard Boselt, Moritz Thurlemann, and Sereina Riniker. Machine learning in qm/mm molecular dynamics simulations of condensed-phase systems. *Journal of Chemical Theory and Computation*, 17(5):2641–2658, 2021.
- [29] Albert Hofstetter, Lennard Bösel, and Sereina Riniker. Graph-convolutional neural networks for (qm) ml/mm molecular dynamics simulations. *Physical Chemistry Chemical Physics*, 24(37):22497–22512, 2022.
- [30] Linfeng Zhang, De-Ye Lin, Han Wang, Roberto Car, and E Weinan. Active learning of uniformly accurate interatomic potentials for materials simulation. *Physical Review Materials*, 3(2):023804, 2019.
- [31] Ryosuke Jinnouchi, Kazutoshi Miwa, Ferenc Karsai, Georg Kresse, and Ryoji Asahi. On-the-fly active learning of interatomic potentials for large-scale atomistic simulations. *The Journal of Physical Chemistry Letters*, 11(17):6946–6955, 2020.
- [32] Justin S. Smith, Benjamin T. Nebgen, Roman Zubatyuk, Nicholas Lubbers, Christian Devereux, Kipton Barros, Sergei Tretiak, Olexandr Isayev, and Adrian E. Roitberg. Approaching coupled cluster accuracy with a general-purpose neural network potential through transfer learning. *Nature Communications*, 10:2930, dec 2019. ISSN 20411723. doi:10.1038/s41467-019-10827-4.
- [33] Alice EA Allen, Nicholas Lubbers, Sakib Matin, Justin Smith, Richard Messerly, Sergei Tretiak, and Kipton Barros. Learning together: Towards foundational models for machine learning interatomic potentials with meta-learning. *arXiv preprint arXiv:2307.04012*, 2023.
- [34] Nima Shoghi, Adeesh Kolluru, John R Kitchin, Zachary W Ulissi, C Lawrence Zitnick, and Brandon M Wood. From molecules to materials: Pre-training large generalizable models for atomic property prediction. *arXiv preprint arXiv:2310.16802*, 2023.
- [35] Justin S Smith, Ben Nebgen, Nicholas Lubbers, Olexandr Isayev, and Adrian E Roitberg. Less is more: Sampling chemical space with active learning. *The Journal of Chemical Physics*, 148(24), 2018.
- [36] Justin S Smith, Roman Zubatyuk, Benjamin Nebgen, Nicholas Lubbers, Kipton Barros, Adrian E Roitberg, Olexandr Isayev, and Sergei Tretiak. The ani-1ccx and ani-1x data sets, coupled-cluster and density functional theory properties for molecules. *Scientific Data*, 7(1):134, 2020.
- [37] Justin S Smith, Olexandr Isayev, and Adrian E Roitberg. Ani-1: an extensible neural network potential with dft accuracy at force field computational cost. *Chemical Science*, 8(4):3192–3203, 2017.
- [38] Masashi Tsubaki and Teruyasu Mizoguchi. Quantum deep descriptor: Physically informed transfer learning from small molecules to polymers. *Journal of Chemical Theory and Computation*, 17(12):7814–7821, 2021.
- [39] Adeesh Kolluru, Nima Shoghi, Muhammed Shuaibi, Siddharth Goyal, Abhishek Das, C Lawrence Zitnick, and Zachary Ulissi. Transfer learning using attentions across atomic systems with graph neural networks (taag). *The Journal of Chemical Physics*, 156(18), 2022.
- [40] Viktor Zaverkin, David Holzmüller, Luca Bonferraro, and Johannes Kästner. Transfer learning for chemically accurate interatomic neural network potentials. *Physical Chemistry Chemical Physics*, 25(7):5383–5396, 2023.
- [41] Michael S Chen, Joonho Lee, Hong-Zhou Ye, Timothy C Berkelbach, David R Reichman, and Thomas E Markland. Machine learning potentials from transfer learning of periodic correlated electronic structure methods: Application to liquid water with afqmc, ccSD, and CCSD(T). *arXiv preprint arXiv:2211.16619*, 2022.

- [42] Silvan Käser and Markus Meuwly. Transfer-learned potential energy surfaces: Toward microsecond-scale molecular dynamics simulations in the gas phase at ccSD (t) quality. *The Journal of Chemical Physics*, 158(21), 2023.
- [43] David Buterez, Jon Paul Janet, Steven J Kiddle, Dino Oglic, and Pietro Lió. Transfer learning with graph neural networks for improved molecular property prediction in the multi-fidelity setting. *Nature Communications*, 15(1):1517, 2024.
- [44] Thorren Kirschbaum and Annika Bande. Transfer learning for molecular property predictions from small data sets. *arXiv preprint arXiv:2404.13393*, 2024.
- [45] John LA Gardner, Kathryn T Baker, and Volker L Deringer. Synthetic pre-training for neural-network interatomic potentials. *Machine Learning: Science and Technology*, 5(1):015003, 2024.
- [46] Maho Nakata and Toshiyuki Maeda. Pubchemqc b3lyp/6-31g**/pm6 data set: The electronic structures of 86 million molecules using b3lyp/6-31g* calculations. *Journal of Chemical Information and Modeling*, 63(18):5734–5754, 2023.
- [47] Surajit Nandi, Tejs Vegge, and Arghya Bhowmik. Multixc-qm9: Large dataset of molecular and reaction energies from multi-level quantum chemical methods. *Scientific Data*, 10(1):783, 2023.
- [48] Horton J, Boothroyd S, Wagner J, Mitchell J, Gokey T, and Dotson D. Open force field bespokefit: Automating bespoke torsion parametrization at scale., 2022.
- [49] Daniel G. A. Smith, Annabelle T. Lolinco, Zachary L. Glick, Jiyoung Lee, Asem Alenaizan, Taylor A. Barnes, Carlos H. Borca, Roberto Di Remigio, David L. Dotson, Sebastian Ehlert, Alexander G. Heide, Michael F. Herbst, Jan Hermann, Colton B. Hicks, Joshua T. Horton, Adrian G. Hurtado, Peter Kraus, Holger Kruse, Sebastian J. R. Lee, Jonathon P. Misiewicz, Levi N. Naden, Farhad Ramezanghorbani, Maximilian Scheurer, Jeffrey B. Schriber, Andrew C. Simmonett, Johannes Steinmetzer, Jeffrey R. Wagner, Logan Ward, Matthew Welborn, Doaa Altarawy, Jamshed Anwar, John D. Chodera, Andreas Dreuw, Heather J. Kulik, Fang Liu, Todd J. Martínez, Devin A. Matthews, III Schaefer, Henry F., Jiří Šponer, Justin M. Turney, Lee-Ping Wang, Nuwan De Silva, Rollin A. King, John F. Stanton, Mark S. Gordon, Theresa L. Windus, C. David Sherrill, and Lori A. Burns. Quantum Chemistry Common Driver and Databases (QCDB) and Quantum Chemistry Engine (QCEngine): Automation and interoperability among computational chemistry programs. *The Journal of Chemical Physics*, 155(20):204801, 11 2021. ISSN 0021-9606. doi:10.1063/5.0059356. URL <https://doi.org/10.1063/5.0059356>.
- [50] Stewart James J.P. Moussa Jonathan E. Mopac, 2024-01-29.
- [51] Christoph Bannwarth, Eike Caldeweyher, Sebastian Ehlert, Andreas Hansen, Philipp Pracht, Jakob Seibert, Sebastian Spicher, and Stefan Grimme. Extended tight-binding quantum chemistry methods. *WIREs Computational Molecular Science*, 11(2):e1493, 2021. doi:<https://doi.org/10.1002/wcms.1493>. URL <https://wires.onlinelibrary.wiley.com/doi/abs/10.1002/wcms.1493>.
- [52] Nathan C Frey, Ryan Soklaski, Simon Axelrod, Siddharth Samsi, Rafael Gomez-Bombarelli, Connor W Coley, and Vijay Gadepally. Neural scaling of deep chemical models. *Nature Machine Intelligence*, 5(11):1297–1305, 2023.
- [53] Joel Hestness, Sharan Narang, Newsha Ardalani, Gregory Diamos, Heewoo Jun, Hassan Kianinejad, Md Mostofa Ali Patwary, Yang Yang, and Yanqi Zhou. Deep learning scaling is predictable, empirically. *arXiv preprint arXiv:1712.00409*, 2017.
- [54] Jared Kaplan, Sam McCandlish, Tom Henighan, Tom B Brown, Benjamin Chess, Rewon Child, Scott Gray, Alec Radford, Jeffrey Wu, and Dario Amodei. Scaling laws for neural language models. *arXiv preprint arXiv:2001.08361*, 2020.
- [55] Xiaohua Zhai, Alexander Kolesnikov, Neil Houlsby, and Lucas Beyer. Scaling vision transformers. In *Proceedings of the IEEE/CVF conference on computer vision and pattern recognition*, pages 12104–12113, 2022.

- [56] Yasaman Bahri, Ethan Dyer, Jared Kaplan, Jaehoon Lee, and Utkarsh Sharma. Explaining neural scaling laws. *arXiv preprint arXiv:2102.06701*, 2021.
- [57] Danny Hernandez, Jared Kaplan, Tom Henighan, and Sam McCandlish. Scaling laws for transfer. *arXiv preprint arXiv:2102.01293*, 2021.
- [58] Diederik P. Kingma and Jimmy Lei Ba. Adam: A Method for Stochastic Optimization. In *3rd International Conference on Learning Representations*, San Diego, CA, USA, May 7-9, 2015.
- [59] Prajit Ramachandran, Barret Zoph, and Quoc V Le. Searching for activation functions. *arXiv preprint arXiv:1710.05941*, 2017.
- [60] Lauri Himanen, Marc O. J. Jäger, Eiaki V. Morooka, Filippo Federici Canova, Yashasvi S. Ranawat, David Z. Gao, Patrick Rinke, and Adam S. Foster. DScribe: Library of descriptors for machine learning in materials science. *Computer Physics Communications*, 247:106949, 2020. ISSN 0010-4655. doi:10.1016/j.cpc.2019.106949. URL <https://doi.org/10.1016/j.cpc.2019.106949>.
- [61] Albert P Bartók, Risi Kondor, and Gábor Csányi. On representing chemical environments. *Physical Review B*, 87(18):184115, 2013.
- [62] Leland McInnes, John Healy, and James Melville. Umap: Uniform manifold approximation and projection for dimension reduction. *arXiv preprint arXiv:1802.03426*, 2018.
- [63] D. G. A. Smith, L. A. Burns, A. C. Simmonett, R. M. Parrish, M. C. Schieber, R. Galvelis, P. Kraus, H. Kruse, R. Di Remigio, A. Alenaizan, A. M. James, S. Lehtola, J. P. Misiewicz, M. Scheurer, R. A. Shaw, J. B. Schriber, Y. Xie, Z. L. Glick, D. A. Sirianni, J. S. O'Brien, J. M. Waldrop, A. Kumar, E. G. Hohenstein, B. P. Pritchard, B. R. Brooks, H. F. Schaefer III, A. Yu. Sokolov, K. Patkowski, A. E. DePrince III, U. Bozkaya, R. A. King, F. A. Evangelista, J. M. Turney, T. D. Crawford, and C. D. Sherrill. Psi4 1.4: Open-source software for high-throughput quantum chemistry. *The Journal of Chemical Physics*, 152(18), 2020.

A Appendix

A.1 Hyperparameters

We employ TorchMDNet2.0 [5] with the same hyperparameters (summarized in table 4) for all datasets and training approaches throughout this work. The only exception is the learning rate, which we reduced from $4 \cdot 10^{-4}$ to 10^{-4} for SpicevL2 for training stability. All training runs were performed on 4 Nvidia A100 GPUs with 8 CPU workers per GPU. The training time of each run varied with the amount of training data, but took less than 5h for ANI1-ccxvL, 1.5 days for QMugsvL, 2.5 days for QM7-XvL, 3 days on SpicevL2.

Table 4: Hyperparameters used throughout this work

Hyperparameter name	value
Initial learning rate (LR)	$3 \cdot 10^{-4}$; 10^{-4} (SpicevL2)
Batch size	28
Optimizer	Adam [58]
LR Scheduler	ReduceLROnPlateau
Decay factor	0.5
Patience	10 epochs
Minimum LR	10^{-7}
StochasticWeightAveraging	LR: 10^{-6}
# Parameters	1.8 million
Cut-off	5 Å
Prediction Heads Hidden Neurons	64
Hidden Channels	128
# Layers	8
# Attention Heads	8
Activation Function	Swish [59]
# RBF	64, Trainable
Neighbor Embedding	True

A.2 Chemical space of the Spicev2 dataset

We split Spicev2 into Spicev1 and Spicev1->2, which cover different parts of chemical space. In order to visualize the shift between these chemical distributions, we use dscribe [60] to compute Smooth Overlap of Atomic Positions (SOAP) [61] descriptors and project them onto a 2-dimensional manifold using the Uniform Manifold Approximation and Projection for Dimension Reduction (UMAP)[62].

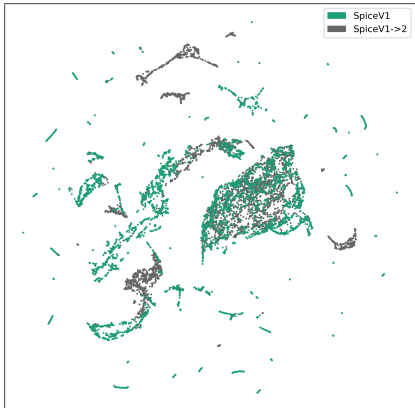


Figure 6: UMAP 2-plot of SOAP descriptors of SpiceV1 and SpiceV1->2

A.3 Performance IDLe versus direct learning for subsets of Spicev1->2

Figure 7 shows the data-efficiency of IDLe GFN2-xTB + PM6 compared to the direct learning baseline. The PubChemv2 and Water Cluster subsets achieve the same accuracy as direct learning using 100% of the HF data. Additionally, the error of IDLe on the Solvated PubChem subset is only marginally larger compared to the baseline. On the other hand, the subsets with larger distribution shift require approx. 25% HF data to reach the 100% HF baseline accuracy. Hence, when generating new data, it appears to be sufficient to label conformers with small to medium distribution shift via SE methods, saving computational budget for HF computations on molecular structures that are highly dissimilar from existing datasets.

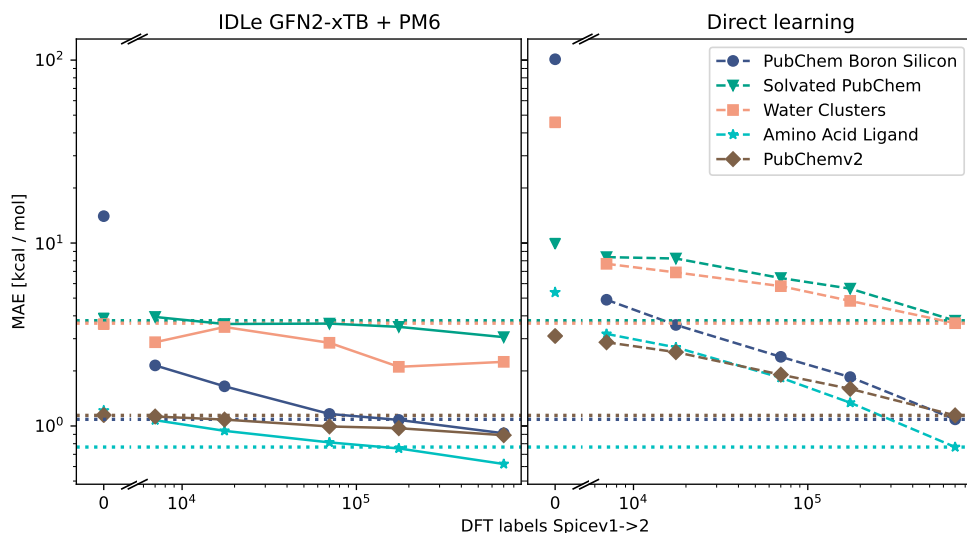


Figure 7: Performance comparison of IDLe GFN2-xTB + PM6 with the direct learning baseline for various subsets of SpiceVL2.

A.4 PubChem-Boron-Silicon subset performance

We separate the PubChem-Boron-Silicon Subset of SpicevL2 from the other 4 subsets of Spicev1->2 given that it is extremely out of distribution (Spicev1 containing no B or Si), resulting in large MAE values in the low data regime for all approaches, which would otherwise dominate the results for the remaining subsets. The main difference to Figure 3 is that all approaches require more data to achieve acceptable accuracy, but the relative performance of the different training approaches is similar.

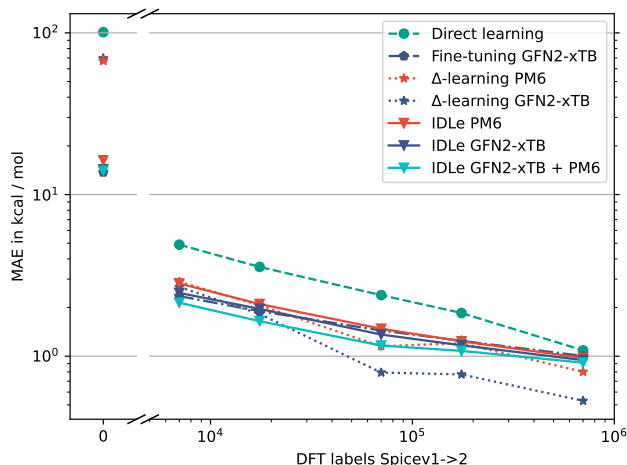


Figure 8: Performance comparison for the PubChem-Boron-Silicon subset of SpicevL2.

A.5 Time benchmarking of various QM methods

We conducted a series of benchmarks on a range of SE, TB, DFT, and CCSD(T) methods to observe the differences in compute time scale required for each method. We selected 17 different small molecules (molecular weights < 250 a.u.), which included some of the most frequently encountered atomic species in the biological field (C, N, O, S, F, Cl) and included three additional small/medium sized solvated system (with molecular weights between 300 and 700 a.u.) to include most of the systems sizes and interaction types covered by the recent *sota* QM datasets. We then correlated the time taken to perform a single point calculation to their exact mass and isotopic molecular weight (Figure 9) and extrapolated this data to obtain the approximate computation of all the datasets in the study (Table 3).

All the benchmarks were executed on an AMD Ryzen Threadripper PRO 3995WX 64-Cores CPU, the calculation were conducted with MOPAC version 22.1.0, XTB version 20.2 for the SE single points label; for the electronic quantum mechanical calculation, the software Psi4 [63] version 1.4.1 was used. All the calculations were run on the backend QCEngine version 0.26.0.

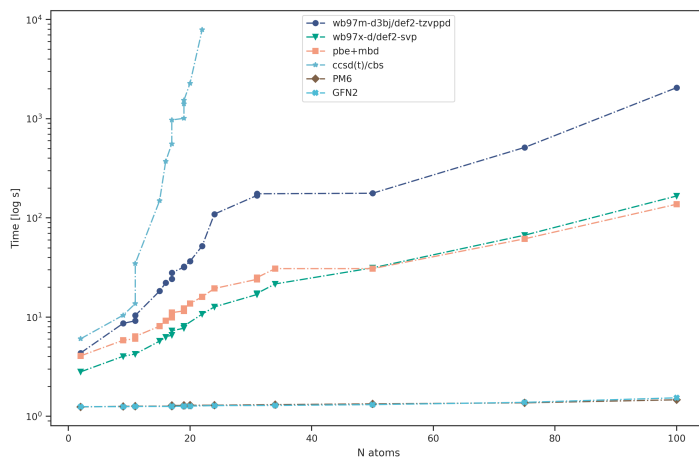


Figure 9: Computational cost of QM computations at various levels of theory scaling with the number of atoms per molecule.

In a realistic setting, most of the selected conformations of the datasets are not only larger but also more complex due to the diversity of interactions involved. For instance, SpiceV2 includes additions of bulk water phases and solvated peptides. This increased complexity would ultimately increase the computation time demanded by high-fidelity DFT methods, extending beyond our initial benchmark results. Consequently, the use of SE/TB calculations and IDLe becomes even more appealing due to their demonstrated efficiency.

A.6 Data scaling coefficients of IDLe on QMugsvL

While the scaling laws of IDLe for increasing HF labels with a fixed amount of LF data follow classical power laws, the scaling behavior when adding conformers with only LF labels is more intricate. Given that the scaling exponent β depends both on the total number of SE and HF labels, we compute the slope of the curves in Figure 5 for each section (vertical gray lines; Table 5). This analysis reveals two distinct trends: lower data efficiency when increasing the number of LF labels a for fixed number of HF labels and higher data efficiency towards adding more LF labels when increasing the amount of HF labels. Thus, when modeling β for scaling LF data, the number of conformers with only LF labels might be more informative than the total number of LF labels.

Table 5: Segment-wise scaling coefficients β on QMugsvL when increasing the percentage of semi-empirical GFN2-xTB labels, for a fixed amount of DFT labels.

DFT labels	GFN2-xTB labels	1% \rightarrow 2.5%	2.5% \rightarrow 10%	10% \rightarrow 25%	25% \rightarrow 100%
	1%		0.257	0.202	0.173
2.5%			0.235	0.190	0.105
10%				0.230	0.151
25%					0.169